Monthly Notices
of the
ROYAL ASTRONOMICAL SOCIETY

Mon. Not. R. Astron. Soc. **422,** 1674–1689 (2012) doi:10.1111/j.1365-2966.2012.20742.x

# A review of source detection approaches in astronomical images

M. Masias,⋆ J. Freixenet, X. Lladó and M. Peracaula

*Department of Computer Architecture and Technology, University of Girona, Campus Montilivi – P-IV building, 17071 Girona, Spain*

Accepted 2012 February 13. Received 2012 February 8; in original form 2011 December 1

**ABSTRACT**

Astronomical images provide information about the great variety of celestial objects in the Universe, the physical processes taking place in it, and the formation and evolution of the cosmos. Great efforts are made to automatically detect stellar bodies in images due to the large volumes of data and the fact that the intensity of many sources is at the detection level of the instrument. In this paper, we review the main approaches to automated source detection. The main features of the detection algorithms are analysed and the most important techniques are classified into different strategies according to their type of image transformation and their main detection principle; at the same time their strengths and weaknesses are highlighted. A qualitative and quantitative evaluation of the results of the most representative approaches is also presented.

**Key words:** methods: data analysis – techniques: image processing.

## 1 INTRODUCTION

The automatic detection of sources in astronomical images seems to be quite a straight-forward task compared to other computer vision problems: the typical scenario is to deal with light-emitting sources on dark backgrounds. Nevertheless, there are some difficulties associated with astronomical image processing that make this task complicated. On the one hand, many astronomical objects do not show clear boundaries since their intensities are similar to the detection levels and they are mixed with the noise component. On the other hand, especially in the case of wide-field deep images showing multiple sources, the sizes and intensities of the different objects present in the images can vary considerably. Therefore the images can have a large dynamic range (i.e. the ratio between the highest and lowest intensity level) and a large spatial dynamic range (i.e. the ratio between the largest and smallest detectable structure). These facts may cause image display problems due to the limited range of intensities perceptible by the human vision system.

Therefore, the main challenge in astronomical object detection is to separate those pixels that belong to astronomical bodies from those that belong to background or noise. Since the goal is to find connected regions of pixels constituting objects, this task is also referred to object segmentation in the computer vision community. Nevertheless, in this document we will often refer to the localization of the central coordinates of the sources as detection. Astronomical detection is usually the first step in the process of building astronomical catalogues. For this reason, after astronomical detection two other processes are also performed: classification, which categorizes the objects into different types (e.g. stars, clusters, galaxies, extended objects, etc.), and photometry, to account for the flux, magnitude or intensity of the objects. The whole process of building a catalogue is also known as source extraction.

The development of automated algorithms for detecting astronomical objects has become a research topic of interest for the astronomical community. Even thought these algorithms perform the same actions that an experienced astronomer can do with an appropriate display system, their importance lies on the fact that the algorithms can do these things quickly, repeatedly and always with the maximum objectivity (properties that a human being cannot guarantee). As stated by Goderya & Lolling (2002), their importance becomes apparent in wide fields or large surveys with thousands of sources that can have intensities at detection levels. In these cases a human search is inefficient, very slow and inaccurate, if not almost impossible.

The first automated methods for astronomical object detection had already been developed in the 1970s, and have evolved until today, although at a relatively slow pace because simple image processing techniques are already used to achieve better results than those performed manually by experts. Nevertheless, more accurate and reliable detection techniques are increasingly required by astronomers, so more complex strategies have been implemented.

We are aware that astronomical imaging is a broad subject and images acquired at different frequency bands present different features and behaviours. However, in this paper we want to give an overview of the most used techniques to find astronomical sources regardless of the origin of the images employed. This does not mean that we obviate the importance of the type of image. By doing this general review we can see whether the techniques perform well with different types of images or if there are more suitable techniques for a specific frequency band.

Although the detection of cosmic bodies in astronomical images has been thoroughly investigated, there are no recently updated surveys covering the whole range of existing strategies. We have to

⋆E-mail: mmasias@eia.udg.edu

go back several years to find a review of astronomical image detection. This may be because in many cases the most important step in astronomical detection is not the detection as such (which can be performed for example with a thresholding process), but image transformation[1] steps such as filtering or deconvolution. These steps are essential to account for or minimize by some percentage unwanted effects (such as noise or interference patterns) introduced by the acquisition sensors.

Bertin (2001) reviewed relevant papers on astronomical source extraction and classification. Regarding the detection processes, mainly focused on optical and near-infrared bands, the author divided the algorithms into two main categories: basic detection algorithms (such as local peak search, thresholding, segmentation, background estimation and filtering) and multi-scale approaches [mainly based on wavelet transforms (WTs)]. Later, Barreiro et al. (2003) compared several filters (such as the Mexican hat wavelet, the matched filter (MF) and the scale-adaptive filter) to optimize source detection using a local peak search. More recently, Starck & Murtagh (2006) devoted some chapters of their book to review some filtering strategies (mainly multi-scale methods such as wavelet and curvelet transforms), deconvolution (e.g. regularized linear methods, Bayesian methods, wavelet-based deconvolution, etc.) and detection [basically a multi-scale vision model (MVM), which we will see later]. Starck & Bobin (2010) also analysed and discussed multi-scale methods based on wavelet, curvelet and ridgelet transforms in astronomical data analysis.

More than 10 years have passed since Bertin (2001) published the last exhaustive review of papers on astronomical image detection. A large number of new strategies have appeared during this last decade, making apparent the lack of an updated review analysing the most recent techniques. Moreover, the innovative techniques developed in fields such as computer vision or machine learning provide more ways to automatically detect astronomical objects in images.

In this paper we review the current state-of-the-art in astronomical source detection, including a detailed analysis of works of this topic, their classification according to the methods used, the image type and the evaluation of their results. We propose a new classification based on two main steps: image transformation and detection criterion. The first one consists in applying changes to the astronomical images to prepare them for the further processing, whereas the second one consists in classifying pixels that belong to sources and separating them from the background pixels, or in finding those pixels where the sources are centred. Moreover, we also analyse the parameters of the strategies reviewed such as the type of images, the reference catalogue, the evaluation measures used and their performance. To the best of our knowledge, this is the first attempt to provide a quantitative and qualitative comparison of the detection approaches according to their reported results in the literature.

The rest of this paper is organized as follows. Section 2 reviews and classifies the image transformation steps used by the analysed approaches. Section 3 shows the classification of the astronomical detection strategies. In Section 4, the measures used to evaluate the results are presented and the performances of the works analysed are compared. The results are discussed in Section 5, and conclusions are drawn in Section 6.

[1] In this paper, the term image transformation refers to all the image processes applied before the actual source detection algorithm. In other fields (e.g. in computer vision), this is also known as pre-processing.

## 2 IMAGE TRANSFORMATION

In this section we review strategies and propose a classification of them according to the type of image transformation they used. In previous reviews there was not such a clear difference between image transformation and detection steps, as the first were considered part of the detection process. Nevertheless, the aims of these two processes are clearly different, and we consider it more appropriate to treat image transformation as a separate group. A summary of the image transformation methods analysed is shown in Table 1.

### 2.1 Image transformation classification

Image transformation is a basic step used to prepare data to achieve a better performance in posterior steps. Before putting into practice some of the image processing steps, some operations may be applied to them to suppress undesired distortions or enhance some features for further processing. Image transformation steps transform raw images in some way, creating new images with the same information content as the original ones, but with better conditions. Thus, the images are adapted to facilitate the posterior analysis, and to obtain better results. In astronomical imaging, the objectives of image transformation are, for instance, to filter the noise, to estimate the background or to highlight the objects.

Within this image transformation group we find techniques such as filtering, deconvolution, transforms or morphological operations. We present a formal and more accurate classification by dividing the image transformation steps into multi-scale strategies, basic image transformations, Bayesian approaches and MF-based strategies. More information is given in Table 1, which presents the image transformation steps and the different works reviewed.

#### *2.1.1 Basic image transformation*

We begin the image transformation review with a range of techniques that, although simple, offer good performance, and hence are widely used throughout the computer vision field. They are basically used to filter noise and to estimate background level.

Simple filtering techniques such as median or average are used by many authors. They consist of a sliding window centred on a pixel that computes one of the statistics mentioned for all the pixels in the window, and finally replaces the central pixel by the computed value (see the example diagram in Fig. 1). For instance, the median filter was used by Damiani et al. (1997) and Makovoz & Marleau (2006) to estimate the background level and to minimize the effect of bright point source light, while Yang et al. (2008), Perret et al. (2008) and Lang et al. (2010) used it to filter noise and smooth the image. With these two aims Herzog & Illingworth (1977), Mighell (1999) and Freeman et al. (2002) used the mean filter. Notice that in some cases pixels in the window with high values are removed to avoid biased values.

Background estimation is a common step in astronomical object detection. A good way to carry it out is the one used in well-known extraction packages such as DAOPHOT (Stetson 1987) and SExtractor (Bertin & Arnouts 1996). Their local background estimation is performed by iteratively applying a thresholding based on the mean and standard deviation to eliminate outliers. Afterwards, a value of the true background is calculated as a function of these statistics (Stetson suggested $3 \times \text{median} - 2 \times \text{mean}$, while Bertin suggested $2.5 \times \text{median} - 1.5 \times \text{mean}$). Some authors refer to this background estimation as $\sigma$-clipping. Others, such as Vikhlinin

**Table 1.** Summary of the analysed astronomical object detection methods according to the image transformation methods, the type of the images and the specified detection aim. The methods are grouped by its image transformation strategy. The acronyms for the detection aim stand for (in alphabetical order): extended source detection (ESD), faint source detection (FSD), point source detection (PSD) and source detection (SD). Notice that the different strategy aims may not be exclusive, but it is just as how the authors referred to it. The term 'N/A' stands for not available information.

| Article | Image transformation | Image type | Aim |
|---|---|---|---|
| | *Basic image transformations* | | |
| Herzog & Illingworth (1977) | Mean | Optical | SD |
| Le Fèvre et al. (1996) | Bijaoui | Multi-band | SD |
| Stetson (1987) | $\sigma$-clipping + Gaussian | N/A | SD |
| Slezak, Bijaoui & Mars (1988) | Gaussian + Bijaoui | Optical | SD |
| Bertin & Arnouts (1996) | $\sigma$-clipping | N/A | SD |
| Szalay, Connolly & Szokoly (1999) | Gaussian | Multi-band | FSD |
| Mighell (1999) | Mean | N/A | SD |
| Hopkins et al. (2002) | Gaussian | Radio | SD |
| Aptoula, Lefèvre & Collet (2006) | Morphological | Multi-band | SD |
| Yang, Li & Zhang (2008) | Median + Morphological | Optical | SD |
| Perret, Lefèvre & Collet (2008) | $\sigma$-clipping + Median + Morphological | Multi-band | SD |
| Haupt, Castro, & Nowak (2009) | Distilled sensing | Radio | SD |
| Lang et al. (2010) | Median | Multi-band | PSD |
| | *Bayesian approaches* | | |
| Hobson & McLachlan (2003) | Markov-chain | N/A | SD |
| Savage & Oliver (2007) | Markov-chain | Infrared | SD |
| Feroz & Hobson (2008) | Nested sampling | N/A | SD |
| Carvalho, Rocha & Hobson (2009) | Multiple posterior maximization | Optical | SD |
| Guglielmetti, Fischer & Dose (2009) | Mixture model | X-ray | SD |
| | *MF* | | |
| Irwin (1985) | Bijaoui + MF | Optical | SD |
| Vikhlinin et al. (1995) | $\sigma$-clipping + MF | X-ray | SD |
| Makovoz & Marleau (2006) | Median + MF | Multi-band | PSD |
| Melin, Bartlett & Delabrouille (2006) | Matched multi-filters | Radio and multi-band | PSD |
| Herranz et al. (2009) | Matched matrix filters | Radio | PSD |
| Torrent et al. (2010) | Boosting | Radio | FSD |
| | *Multi-scale approaches* | | |
| Bijaoui & Rué (1995) | Wavelet | Optical | SD |
| Kaiser, Squires & Broadhurst (1995) | Mexican Hat | Multi-band | SD |
| Damiani et al. (1997) | Gaussian + Median + Mexican Hat | X-ray | SD |
| Starck et al. (1999) | Wavelet | Mid-infrared | FSD |
| Lazzati et al. (1999) | $\sigma$-clipping | X-ray | SD |
| Freeman et al. (2002) | Mean + Mexican Hat | X-ray | SD |
| Starck (2002) | Wavelet + Ridgelet | Infrared | SD |
| Starck, Donoho & Candès (2003) | Wavelet + Curvelet | Infrared | SD |
| Vielva et al. (2003) | Mexican Hat (spherical) | Radio | PSD |
| Belbachir & Goebel (2005) | Contourlet + Wavelet | Infrared | FSD |
| Bijaoui et al. (2005) | Wavelet + PSF smoothing | Multi-band | SD |
| González-Nuevo et al. (2006) | Mexican Hat (family) | Radio | PSD |
| Starck et al. (2009) | Multi-scale variance stabilization | $\gamma$-ray | SD |
| Peracaula et al. (2009b) | Gaussian + Wavelet | Radio | PSD |
| Peracaula et al. (2011) | Gaussian + Wavelet | Radio and infrared | ESD |
| Broos et al. (2010) | Wavelet | X-ray | SD |

et al. (1995), Lazzati et al. (1999) and Perret et al. (2008), also used this method to deal with the background estimation.

Some authors (Irwin 1985; Slezak et al. 1988; Le Fèvre et al. 1996) mentioned that they used a method that Bijaoui (1980) presented more than 30 years ago. It was based on a Bayesian estimation of the intensity at each point using the histogram of the densities. A model of this histogram was then built, taking into account the granulation and the signal distribution, and obtaining the

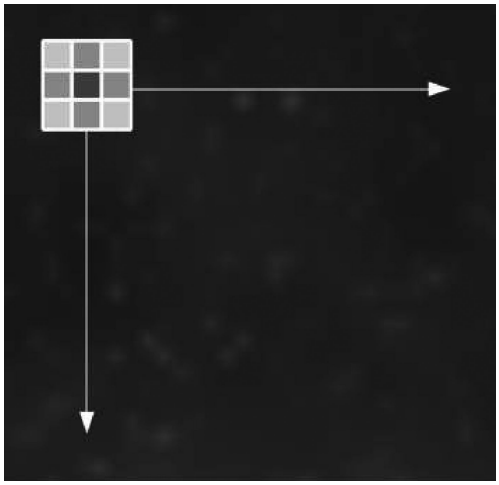

**Figure 1.** A simple diagram of how filtering works. A specific filter is convolved to the image.

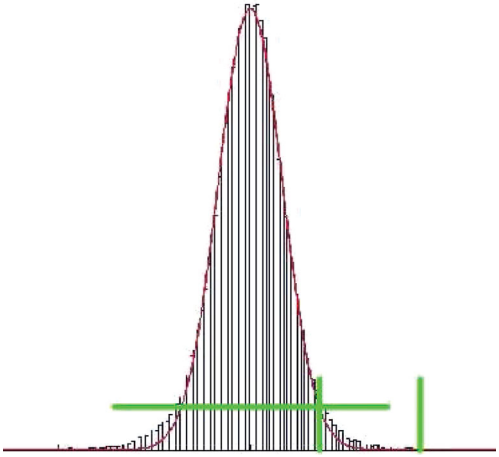

**Figure 2.** An example of Gaussian fitting of an intensity histogram where the two values marked with vertical lines represent noise and source intensity levels.

best threshold to separate the sky from the foreground. Although at first it was a widely used background estimation strategy, it became less common due to its high computational cost.

Sometimes, when the background presents large variations or the noise level is high, a background subtraction is applied (Slezak et al. 1988; Le Fèvre et al. 1996). After the subtraction, the source detection process becomes easier. The background subtraction is usually performed from the background estimation, removing those pixels considered as background. Haupt et al. (2009) developed a different method called distilled sensing, which was based on the idea of ruling out the regions where the signal (sources) was not present, and then focusing on the rest of regions. They perform iterative thresholding to discard regions where the signal was absent, and then the source detection was intensified in the regions not discarded.

Another common image transformation step is to convolve the image with a Gaussian profile. In optical imaging, this process can be understood as an approximation to model the point spread function (PSF; the response of the acquisition instrument to a point source) to the image pixels, thereby obtaining a new map with the probability that each pixel has to be part of an object. Gaussian fitting can be computed by subtracting the mean of the sky and dividing it by the Gaussian deviation. As Stetson (1987) mentioned, Gaussian fitting is equivalent to going through each pixel and considering the expected brightness each one should have when an object is centred on it. A numerical answer to this question is estimated by fitting a Gaussian profile: if a star is truly centred on that pixel, it becomes a positive value proportional to the brightness of the object. Otherwise, the pixel value becomes close to zero or negative. Szalay et al. (1999) and Hopkins et al. (2002) also applied this strategy to multi-band and radio frequency images. Moreover, Damiani et al. (1997) in their multi-scale approach applied a Gaussian filter to the image in order to smooth the spatial variations of the background. Slezak et al. (1988) also applied this convolution to optical images in order to enhance very faint objects.

Furthermore, Gaussian models may also be used to filter noise. Modelling the intensity of the image pixels as a Gaussian, the bell-shaped zone may be considered as noise, while the rest of the distribution may represent background and objects. This noise filtering by Gaussian fitting of the histogram was used by Slezak et al. (1988), and more recently by Peracaula et al. (2009b, 2011). Fig. 2 shows a Gaussian fitting of a histogram.

Morphological operations are another typical image transformation step used in computer vision. A generalization to grey-scale images allows the morphological image transformation step to be applied in this type of images. The two main operations in morphology are dilation and erosion. In binary images, white pixels are considered foreground, and black pixels are considered background. As its name suggests, dilation expands white pixels, replacing the patch around the pixel with a given structural element (SE; a mask with a specific shape), while erosion compresses the foreground by replacing a patch that matches with the SE for a unique white pixel. In other words, dilation adds pixels to the foreground edges, while erosion removes pixels from the edges. The combination of dilation and erosion (in this order) is called 'close' operation, whereas the inverse process is called 'open' operation. In grey-scale morphology, SEs are defined as functions.

The works that have used morphological grey-scale image transformation step include Aptoula et al. (2006) and Yang et al. (2008), who filtered the noise and enhanced the image by computing open and close operations. Another work based on morphology is Perret et al. (2008). They proposed the use of the grey level hit-or-miss transform (HMT). The HMT is a morphological operator dedicated to template matching that uses an erosion and a pair of disjoint structuring elements. In this transform, the image is convolved with two different SE types: while the first one is used to match the object shape (foreground), the second one is used to match the spatial neighbourhood of this shape (background). In the approach of Perret et al. (2008), the SE corresponding to foreground and background are patches of objects with variations in orientation and elongation convolved with a Gaussian filter to simulate the PSF. A different grey level according to the background estimation is given to these patches to get, on the one hand, the foreground SE, and, on the other hand, the background SE. After background estimation and noise filtering, the two SEs are convolved with the image and the output score image can easily be thresholded.

### *2.1.2 Bayesian approaches*

The goal of these approaches is to prepare the data in order to establish the probability that it is either object or background. In other words, the objective is to provide a probability map with higher values in the zones where an astronomical object is more likely to

be located, and lower values in the zones that are more likely to be sky. Bayesian approaches are based on the widely used Bayesian inference, where a set of evidence or observations is used to update the probability that a hypothesis is true. Bayesian inference tries to estimate the values of a set of parameters $O$ in some reasonable model (or hypothesis) of the data (in our case, the image) $I$. For any given model, an expression of the probability of obtaining the data set given a particular set of values for the parameters (this is the so-called likelihood) must be considered. Moreover, a prior probability of the parameters based on some knowledge regarding their values before analysing the data must be imposed. The Bayesian approach consists in constructing the conditional probability density relationship:

$$p(O|I) = \frac{p(I|O)p(O)}{p(I)}, \quad (1)$$

which gives the posterior distribution $p(O|I)$ in terms of the likelihood $p(I|O)$, the prior $p(O)$ and the evidence $p(I)$.

For the purpose of estimating parameters, the evidence is usually set to a constant value, so it is usual to talk about un-normalized posterior distribution. It is called maximum a posteriori (MAP) solution, and we can see it as a maximization over $O$ that involves a maximum likelihood and a prior:

$$\mathrm{MAP}(O) = \max_O p(I|O)p(O). \quad (2)$$

If we are able to assess the likelihood, then (after applying a prior) we will be able to have the posterior probability, which is the final resulting image. It expresses the probability of the data $I$ given any particular set of parameters $O$. In practice, the likelihood is often based on an exponential function that involves the data (the different pixels), the signal contribution and the noise model (Gaussian, Poisson, etc.).

Referring to the prior knowledge, noise characteristics and the PSF can be used. Any other fit parameters can also be assumed. For example, source position and amplitude may have already been determined in another observing band. More information about Bayesian methodology is available in Starck & Murtagh (2006) and Hanson (1993).

Hobson & McLachlan (2003) studied two alternative strategies to detect discrete objects: the simultaneous detection of all the discrete objects in the image, and the iterative detection of objects one by one. In both cases, the parameter characterization of the objects of interest was carried out by means of Markov-chain Monte Carlo sampling (MCMC) [see Hobson & McLachlan (2003), Savage & Oliver (2007), and references therein to know more about MCMC]. Using MCMC they could sample numerically from an unnormalized posterior distribution. They used as prior knowledge the mean estimation of the number of objects per image (an empirical value). For instance, in the iterative detection method proposed by Hobson & McLachlan (2003), this value was set to 1, because it was the number of objects to be found at each iteration. In a similar way, Savage & Oliver (2007) developed a filter to source detection (and a simultaneous background estimation) in infrared images. Moreover, using MCMC they tried to determine the related probability at each pixel of being described by two different models: empty sky and point source against a uniform background. Calculating the maximum posterior value for each model (using the PSF as prior knowledge), a map with the probability of where a point source was more likely to be located was generated.

On the other hand, Feroz & Hobson (2008) followed the Hobson & McLachlan (2003) approach, but they replaced the MCMC by another Monte Carlo technique, nested sampling. They used it to calculate the posterior distribution as a by-product. In a similar way, and also following the Hobson & McLachlan (2003) approach, Carvalho et al. (2009) proposed an object detection method called PowellSnakes, computationally faster than Bayesian methods based on MCMC. In their approach, sampling was skipped and the detection method was directly applied to the posterior. An estimation of position, amplitude and spatial shape of sources was estimated in order to be used as prior knowledge. Guglielmetti et al. (2009) applied their Bayesian source detection method to X-ray images. They used two different kinds of prior knowledge: exponential and inverse-Gamma function as probability density functions of sources, and two-dimensional thin plate splines (TPS; see references in Guglielmetti et al. 2009) to represent the background.

### 2.1.3 *Matched filtering*

The purpose of applying a filtering step is to highlight objects and reduce the background fluctuations. The most commonly used filter to solve these two problems is the MF. This filter convolves the image with the profile of the objects that are expected to be found (e.g. PSF for point source detection or other patterns for extended source detection). A simple example of how it works is shown in Fig. 3. In addition, the MF may be used to subtract the background locally, and it is also a filter to consider when the images present a considerable amount of noise.

Many authors have proposed filtering raw images with an MF before applying a method to detect the objects. In the 1980s, Irwin (1985) suggested the use of the seeing function as an MF to detect faint sources in a noisy background. The seeing function can be obtained either by directly averaging suitable stellar profiles or by an analytic model fit to these profiles. A background estimation [following the Bijaoui (1980) method] was also computed previously to correct spurious values and to homogenize the sky. The MF allowed the signal-to-noise ratio (SNR) to be increased, so the sources and the background were easily separated by a thresholding.

Vikhlinin et al. (1995) proposed a similar strategy focused on X-ray data that, first of all, generated a background map using a sliding box thresholding that detected the brightest sources for removal. Afterwards, an MF defined as a piecewise function was applied to the residual image. Depending on two thresholds (obtained with the background estimation), the current pixel was convolved with a different function branch in order to differentiate sources and

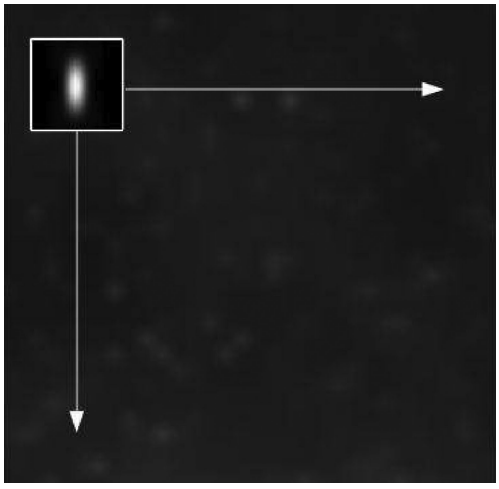

**Figure 3.** A simple diagram of the matched filtering. A profile of the expected sources to be found is convolved to the image.

background. Pixels that were source candidates were convolved with the instrument PSF, whereas pixels that were background candidates were convolved so that their values were zero or negative. Thus, a detection method could be applied to the resulting image. This process is repeated iteratively until a stop criterion is reached.

Another approach based on MF was developed by Makovoz & Marleau (2006). It was included in the MOPEX package for astronomical image processing. To detect point sources, first and foremost, the background was subtracted from the image by locally calculating the median, and subtracting it from the current pixel. Then, an MF based on point response function (PRF) was applied to the background-subtracted image. With the background subtraction step, some bright sources could be extracted, and using patches of these sources, the PRF could be estimated. The detection process was repeated iteratively, so the PRF could be refined with the new sources extracted.

In the literature, some authors have also used MF with multi-band images, the so-called matched multi-filters. For example, Melin et al. (2006) used this extension of the MF to detect clusters. Each band was convolved with the corresponding filter (they used the knowledge of the cluster signal, such as its spatial and spectral features at each band), and a unique filtered image was produced by combining all filtered bands. In a similar way, Herranz et al. (2009) introduced what they called matrix filters (or matched matrix filters). The main difference was that they convolved each band with its corresponding filter, but a filtered image per band was generated so a final choice of which filtered bands were better to perform the detection step was needed.

In a recent work, Torrent et al. (2010) detected faint compact sources in radio frequency images using a machine-learning technique that follows the main principles of matched filtering. First of all, a set of local features (patches of faint sources) was extracted from different images convolved with a bank of filters, making the so-called dictionary. Afterwards, the images were divided into two sets: training and testing. The images of these two sets were characterized by convolutions with the bank of filters and with cross-correlations with the dictionary images, thereby obtaining probability images with high values in the regions similar to the patches. Finally, a boosting classifier (Freund & Schapire 1997; this algorithm is based on the simple idea that the sum of weak classifiers can produce a strong classifier) was trained with the training set and the detection was performed in the testing set images.

### 2.1.4 Multi-scale approaches

In computer vision, the concept of multi-scale (or multi-resolution) is often used when the image to be segmented shows objects with very different sizes or patterns organized in a hierarchical structure. In astronomical image processing, multi-scale approaches have been extensively used during the last 15 years, mainly because in many cases, they outperform other strategies based on more basic techniques.

Astronomical data generally have a complex hierarchical structure, and for this reason a more suitable way to represent it is in the multi-scale space. Thus, images are decomposed into components at different scales (different spatial frequencies), and objects become highlighted in some scales. Depending on the nature of the objects, they may appear in more or less scales, and closer to low or high frequency scales. Once the decomposition is complete, a basic detection algorithm can be applied in different scales, as if they were single-scale images.

In other words, multi-scale strategies optimize the analysis and detection of astronomical objects, however complex they may be. Among their applications, we find denoising, source deblending (an astronomy technique to isolate overlapped sources) and inpainting (the process of reconstructing missed or deteriorated parts of images), among others.

Several multi-scale decompositions are used in the literature, the WT being the most used by far. This transform and other multi-scale approaches focused on the detection of astronomical objects are commented below. See Graps (1995) and Starck & Murtagh (2006) for a more detailed description of wavelets and other multi-scale transforms.

*2.1.4.1 The wavelet transform* If we deal with multi-scale astronomical imaging, we cannot avoid mentioning the WT. It is the common multi-scale technique used in the MVM (Bijaoui & Rué 1995) that we will see later. The most used transform is the stationary wavelet transform (SWT), more commonly known as 'à trous' algorithm (which is the French translation of holey, which means that zeros are inserted in the filters), an extension of the discrete WT designed to overcome the lack of shift-invariance. Since astronomical sources are mostly isotropic (such as stars) or quasi-isotropic (such as galaxies or clusters), the SWT does not favour any direction in the image and maintains the sampling at each scale.

The SWT of a signal produces $N$ scales $W_n$, and each scale is composed of a set of zero-mean coefficients. Moreover, a smoothed array is generated using a smoothing filter $h$ (associated with the wavelet scaling function) in the following way:

$$I(i,j) = F_N(i,j) + \sum_{n=1}^{N} W_n(i,j), \tag{3}$$

where $I(i, j)$ refers to the intensity of the pixel in the raw $i$ and column $j$ of the image $I$. $F_N(i,j)$ and $W_n(i,j)$ are calculated through the following iterative process:

$$\begin{aligned} F_0(i,j) &= I(i,j) \\ F_n(i,j) &= \langle H_n, F_{n-1}\rangle(i,j) \\ W_n(i,j) &= F_{n-1}(i,j) - F_n(i,j) \end{aligned} \tag{4}$$

with $n = 1, ..., N$ and

$$\langle H_n, F_{n-1}\rangle(i,j) \equiv \sum_{k,l} h(k,l) F_{n-1}(i + 2^{n-1}k,\, j + 2^{n-1}l). \tag{5}$$

The set $W_1, W_2, ..., W_N$ together with $F_N$ represents the WT of the image as can be seen in Fig. 4.

The discrete filter $h$ is derived from the scaling function and, as suggested by Starck & Murtagh (2006), a good choice for $h$ is to use a spline of degree 3, and therefore, the mask associated with the filter takes the following form:

$$h \equiv \frac{1}{256}\begin{pmatrix} 1 & 4 & 6 & 4 & 1 \\ 4 & 16 & 24 & 16 & 4 \\ 6 & 24 & 36 & 24 & 6 \\ 4 & 16 & 24 & 16 & 4 \\ 1 & 4 & 6 & 4 & 1 \end{pmatrix}. \tag{6}$$

There are many extensions of the WT that are more suitable depending on the detection goal. For example, Damiani et al. (1997) proposed a method based on the Mexican hat wavelet transform (MHWT – a special case of the family of continuous wavelets obtained by applying the Laplacian operator to the 2D Gaussian;

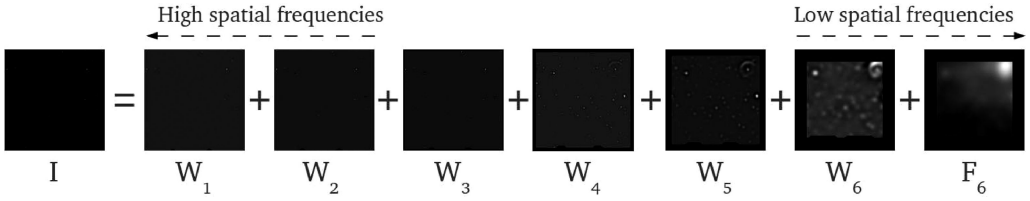


**Figure 4.** A six-scale wavelet decomposition.

for more information about it see Kaiser et al. (1995); Carvalho et al. (2009); Freeman et al. (2002) and references therein) to detect sources in X-ray images. Moreover, this kind of WT was used by other authors, such as Vielva et al. (2003), who used the spherical MHWT (an MHWT extension for spherical functions) to detect point sources in all-sky radio frequency maps. More recently, Starck et al. (2009) proposed a source detection approach based on the multi-scale variance stabilization transform (MSVST; based on differences of two consecutive WT scales) applied to gamma-ray images. Kaiser et al. (1995) pioneered the use of WT for astronomical object detection. Specifically, they used the MHWT in multi-band images to highlight faint objects.

As the image transformation and the detection in multi-scale approaches are closely linked, and sometimes one step overlaps the other, more information about these methods can be obtained in Section 3.1.3.

*2.1.4.2 Multi-scale decomposition for anisotropic data* While wavelets have good performance with isotropic features, they are far from optimal with anisotropic objects. Because of this, the astronomical community has had to find alternatives. Some multi-scale methods that represent the anisotropic features well have been demonstrated.

To overcome the weakness of wavelets in anisotropic data, Candès & Donoho (1999, 2000) proposed two new methods of multi-scale representation: curvelet and ridgelet transforms, which are very different from wavelet-like systems. Curvelets and ridgelets take the form of basic elements that exhibit high directional sensitivity and are highly anisotropic. For instance, in two dimensions, curvelets are localized along curves, in three dimensions, along sheets, etc. The ridgelet transform can effectively deal with line-like phenomena in two dimensions, plane-like phenomena in three dimensions, and so on. More details on these two techniques are provided in Starck & Murtagh (2006).

In practice, the continuous ridgelet transform (CRT) is used. The idea is to apply the Radon transform (see Candès & Donoho 1999, and references therein) and perform a wavelet analysis in the Radon domain. Thus, the image is represented as functions with simple elements that are in some way related to ridge functions. CRT is therefore optimal to detect lines and segments in images.

Curvelets are also an extension of the wavelet concept. The idea of the curvelet transform is to first decompose the image in different scales, and then analyse each scale by means of a local ridgelet transform. They have strong directional character in those elements that are highly anisotropic at fine scales. Hence, for specific astronomical data containing edges (planet surfaces, for example), curvelets are the best choice because they provide a mathematical representation that is ideally adapted to represent objects with curved shapes.

As sometimes both isotropic and anisotropic data are present in images, combined approaches may be the best solution. Hence, a perfect multi-scale decomposition should benefit from both the wavelet advantages and the ridgelet or curvelet transforms (or maybe others) as well. In practice, these combined approaches are actually used, instead of curvelets or ridgelets alone. For instance, Starck (2002) and Starck et al. (2003) proposed, on the one hand, combinations of wavelets and ridgelets and, on the other hand, combinations of wavelets and curvelets to detect objects in infrared data. In an another work, Belbachir & Goebel (2005) suggested the combined use of WT and contourlet [see the Belbachir & Goebel (2005) paper and references therein] for faint source detection also in infrared images. Contourlet is a filter bank transform that can deal with smooth images with smooth contours, so it is similar to the curvelet transform.

### 2.2 Image transformation for anomalous data correction

Besides noise, there are other harmful effects directly related to the acquisition instruments which may complicate the detection process. For example, pixels in astronomical images are sometimes missing or corrupt (also known as dead pixels), causing some difficulties. Hence, the automated detection approaches should be robust to them in the sense that the detection performance should not differ dramatically in the presence of anomalous image data.

Basic image transformation techniques such as simple filtering are used to reduce the impact of outliers. For instance, average deviation and median filtering are used for this purpose (Starck & Murtagh 2006). $\sigma$-clipping is another robust basic image transformation used with anomalous data as shown by Zhang (1995).

Zhang, Luo & Zhao (2004) reviewed several methods to detect outliers in astronomical images. They classified these methods into different categories: distribution-based, where a standard distribution is fit to the data and pixels that are far from the median are considered outliers; depth-based, where pixels that are out from different convex hulls are considered as outliers; distance-based, where pixels that are away from a certain specified distance are considered as outliers; density-based, where outliers are identified as those pixels that are significantly different from their neighbours; or clustering-based, where outliers are grouped according to a certain criterion. They highlighted some advantages and drawbacks of the different categories. For example, they mentioned that distance-based methods are efficient finding outliers, while distribution-based and depth-based have a high computational cost. Moreover, they stated that density-based methods are more appropriate when images present different types of outliers, and clustering-based methods do not perform well with noisy images.

Other common practices used to deal with missing and corrupted data are based on image reconstruction or deconvolution. For example, Haindl & Šimberová (1996) mentioned several ways to reconstruct corrupted image data such as replacing them by adjacent data, interpolating among the surrounding data, using template replacement (replacing the corrupted data by data from a similar available band) or applying regressions. These techniques have been used

in the astronomical imaging field but have also gained importance during the last years in other domains of the image processing and computer vision, being referred often as image inpainting (Bertalmio et al. 2000; Criminisi, Pérez & Toyama 2004). As stated by Starck & Bobin (2010) the application of multi-scale methodologies such as the WT may be seen also as an inpainting technique.

## 3 DETECTION CRITERIA

After presenting the image transformation techniques, in this section we analyse the different strategies used to detect sources. We propose a classification of them as can be seen in Table 2.

**Table 2.** Summary of the analysed astronomical object detection approach according to the detection methods, the type of the images and the specified detection aim. The methods are grouped by the way they perform the detection. The acronyms for the detection aim stand for (in alphabetical order): extended source detection (ESD), faint source detection (FSD), point source detection (PSD), and source detection (SD). Notice that the different strategy aims may not be exclusive, but it is just as how the authors referred to it. The term 'N/A' stands for not available information.

| Article | Strategy | Image type | Aim |
|---|---|---|---|
| | *Thresholding* | | |
| Jarvis & Tyson (1981) | Local | Optical | FSD |
| Irwin (1985) | Global | Optical | SD |
| Le Fèvre et al. (1996) | Local | Multi-band | SD |
| Slezak et al. (1988) | Global | Optical | SD |
| Bijaoui & Rué (1995) | Global | Optical | SD |
| Bertin & Arnouts (1996) | Global | N/A | SD |
| Szalay et al. (1999) | Global | Multi-band | FSD |
| Starck et al. (1999) | Global | Mid-infrared | FSD |
| Lazzati et al. (1999) | Global | X-ray | SD |
| Hopkins et al. (2002) | Global | X-ray | SD |
| Freeman et al. (2002) | Global | X-ray | SD |
| Makovoz & Marleau (2006) | Global | Multi-band | PSD |
| Melin et al. (2006) | Local | Radio and multi-band | PSD |
| Yang et al. (2008) | Local | Optical | SD |
| Herranz et al. (2009) | Global | Radio | PSD |
| Starck et al. (2009) | Global | Gamma-ray | SD |
| Peracaula et al. (2009b) | Local | Radio | PSD |
| Haupt et al. (2009) | Global | Radio | SD |
| Peracaula et al. (2011) | Local | Radio and infrared | ESD |
| Torrent et al. (2010) | Local | Radio | FSD |
| Lang et al. (2010) | Global | Multi-band | PSD |
| | *Local peak search* | | |
| Herzog & Illingworth (1977) | Detection threshold | Optical | SD |
| Newell & O'Neil (1977) | Detection threshold | Optical | SD |
| Kron (1980) | Profile fitting | Multi-band | FSD |
| Buonanno et al. (1983) | Detection threshold | Multi-band | SD |
| Stetson (1987) | Profile fitting | N/A | SD |
| Vikhlinin et al. (1995) | Detection threshold | X-ray | SD |
| Kaiser et al. (1995) | N/A | Multi-band | SD |
| Damiani et al. (1997) | Detection threshold | X-ray | SD |
| Mighell (1999) | Profile fitting | N/A | SD |
| Vielva et al. (2003) | N/A | Radio | PSD |
| Hobson & McLachlan (2003) | Profile fitting | N/A | SD |
| López-Caniego et al. (2005) | Profile fitting | N/A | PSD |
| González-Nuevo et al. (2006) | N/A | Radio | PSD |
| Savage & Oliver (2007) | Profile fitting | Infrared | SD |
| Feroz & Hobson (2008) | Profile fitting | N/A | SD |
| Carvalho et al. (2009) | Profile fitting | Optical | SD |
| Broos et al. (2010) | N/A | X-ray | SD |
| | *Other methods* | | |
| Andreon et al. (2000) | Neural networks | Multi-band | SD |
| Liu, Chiu & Xu (2003) | Neural networks | Multi-band | SD |
| Aptoula et al. (2006) | Watershed transform | Multi-band | SD |
| Peracaula et al. (2009a) | Contrast radial function | Radio | FSD |
| Perret, Lefèvre & Collet (2010) | Connected component trees | Multi-band | SD |

### 3.1 Detection criteria classification

Image transformation techniques provide a new image or map ready to be processed. At this point, a detection method is ready to be applied to the images. The goal of detection is to locate the astronomical objects and separate them from the background (the sky). Two detection strategies stand out among the rest: thresholding and local peak search. Thresholding considers that connected pixel regions above a certain threshold belong to an object, whereas local peak search finds those pixels that are maximums in a pixel neighbourhood and, from this point, tries to find all the object pixels. Even though these two methods are the most common, we also analyse other strategies that try to solve the detection problem in different ways (most of these strategies are relatively recent). More information is available in Table 2, which shows the detection strategies used in the various works analysed.

#### *3.1.1 Thresholding*

In computer vision, thresholding is a simple method for image segmentation. Using this method, a grey-scale image is converted to a binary one where the pixels have only two possible values: 0 or 1. These two values are assigned to pixels whose intensities are below (0) or above (1) a specified threshold. In astronomical images (and in many other fields), thresholding is used to decide which regions (connected pixels) are considered as objects and which are considered as background. In a more formal way, the binarized image $I_{\rm th}$ is the result of applying the following function to all the pixels of the original image $I$:

$$I_{\rm th}(i,j) = \begin{cases} 1 & \text{if } I(i,j) > \text{th} \\ 0 & \text{otherwise,} \end{cases} \tag{7}$$

where $I_{\rm th}(i, j)$ and $I(i, j)$ is the intensity of the pixels in row $i$ and column $j$ of the binarized and original images, respectively, and th is the established threshold.

Defining an appropriate threshold is not easy due to several factors like noise, background variations or diffuse edges of the objects. Any chosen threshold may result in some true objects being overlooked (false negatives) and some spurious objects being considered as real (false positives). Varying the threshold to the extremes minimizes one of these types of errors, but maximizes the other. Hence, the difficulty lies in setting the threshold to get the two errors as small as possible.

In the reviewed papers, the authors have set the threshold following several strategies. For example, Irwin (1985) and Freeman et al. (2002) set it depending on the sky estimation computed, while Starck et al. (1999, 2009) and Lang et al. (2010) set it depending on the noise (as a multiple of the noise estimation). Szalay et al. (1999) modelled the sky as a $\chi^2$ distribution, and got the threshold value in the intersection point between the theoretical distribution and the real data distribution. In a different way, Slezak et al. (1988) and Herranz et al. (2009) determined the threshold by the distribution of the peaks previously found. They set the threshold at 3.8 and 5 times the deviation of the peak distribution, respectively. Hopkins et al. (2002), moreover, used the false discovery rate (FDR) method to select a threshold that controls the fraction of false detections (see the Hopkins paper for more information). Haupt et al. (2009) also used a threshold obtained through FDR after ruling out regions without sources with their distilled sensing method. In a similar way, Lazzati et al. (1999) obtained the threshold as a function of the number of pixels, the background estimation and the maximum number of spurious sources expected.

However, not all the methods are fully automated. Source extraction packages such as SExtractor (Bertin & Arnouts 1996) and mopex (Makovoz & Marleau 2006) used user-specified thresholds (e.g. SExtractor gives the possibility of setting the threshold to an absolute value or as a multiple of the background level). In these tools, when a source is considered too large, it may be assumed to be a cluster of sources, and the threshold is raised to detect the sources independently.

Mainly due to the background variations, a common practice in astronomical image detection is local or adaptive thresholding: a different threshold is used for different regions in the image. It can typically be computed using a sliding window. For example, Jarvis & Tyson (1981) adapted the threshold as the window progresses. Starting with a specific threshold, if pixels in the window were lower than the threshold (and so were considered as sky), the threshold value was updated with the sky value of these pixels. Another way to fix the threshold locally was the way Le Fèvre et al. (1996) did it. They computed the histogram of pixel intensities at each window, and set the threshold at 1.5 times the deviation distribution. Other approaches have recently been proposed by Peracaula et al. (2009b, 2011) and Torrent et al. (2010), who defined the local threshold by means of the local noise determined by the pixel intensity histogram, or by Melin et al. (2006), who used a multiple value of the SNR. Yang et al. (2008) used a method to automate threshold calculation called the Otsu method (Otsu 1979), where the intra-class variance is minimized to get a good threshold.

#### *3.1.2 Local peak search*

The main principle of the local peak (or maxima) search method consists in searching those pixels that are considered peaks or, in other words, that are a local maximum in a neighbourhood. In most cases, to avoid the unnecessary analysis of all the pixels, only those peaks that are above a given threshold are considered. When this detection method is used, it is often accompanied by an image transformation step that enhances the peaks to be found, and another step computed after the peak search that establishes or corrects the pixels around the peak that belong to the object. Many times, this last step is a fitting process, which is possible because the nature of the objects is well known. So the local peak search as such provides a list of candidates that can be the central points of an object. For this reason, this method is typically used as the step previous to photometry calculation. The local peak search is more appropriate to detect stars and other point sources, and is not well suited to detect complex objects (like galaxies and other extended sources). A formal representation of this method is as follows:

$$I_{lps}(i,j) = \begin{cases} 1 & I(i,j) \geq I(k,l) \\ 0 & \text{otherwise,} \end{cases} \tag{8}$$

where $I(i, j)$ is the intensity of the pixels in row $i$ and column $j$, and $I(k, l)$ is the intensity of a neighbour pixel of $I(i, j)$. For example, considering an eight-connectivity (described below), $k$ takes values from $i - 1$ to $i + 1$, and $l$ takes values from $j - 1$ to $j + 1$.

This method was already used in the late 70s by Herzog & Illingworth (1977) and Newell & O'Neil (1977). They defined a peak as a pixel with an intensity greater than or equal to their eight adjacent pixels (eight-connectivity) and over a threshold based on the sky level computed. Therefore, the objects were the connected regions centred on a peak. They conducted some tests to deblend objects

(connected regions with more than one peak), such as data over gradient (DOG) test (see Herzog & Illingworth 1977; Newell & O'Neil 1977 and references therein for more information about this test). Moreover, Buonanno et al. (1983) searched peaks over the sky level (in windows of $N \times N$), and all the pixels connected to the peaks above a certain threshold were added to make the corresponding objects. Vikhlinin et al. (1995), in X-ray images, considered a pixel as maximum if it was greater than its 25 neighbours and also above a threshold (based on the background).

In several approaches, once the peaks were found, a known distribution around them was fit. In this sense, Kron (1980) opened windows of 50 × 50 around the maximums found, computed the histograms and selected the distribution (between two different light distributions that model faint and bright sources) that best fits the histograms. In a similar way, Savage & Oliver (2007) opened a window for each peak in infrared images and selected the distribution (among sky, point-shaped source or extended source) that best fits. López-Caniego et al. (2005) searched for local maximums and distinguished the ones caused by the presence of sources. This distinction was achieved by a constrained optimization problem that considered peak densities leading to an optimal distribution that fits the source in amplitude and curvature. Other works used sharpness and roundness statistics and PSF fitting (Stetson 1987 in its DAOPHOT software), or analysed the annulus surrounding the peaks to determine what was background and what was source (Mighell 1999).

### 3.1.3 *Multi-scale vision model*

The multi-scale transform by the 'à trous' algorithm decomposes an image $I(i, j)$ in $N$ scales or wavelet planes $w_n(i, j)$. Thus, a detection method can be independently applied to each of these images representing a scale. Each scale has the same number of pixels as the image. As we have already mentioned, the original image can be expressed as the sum of all the wavelet scales and the smoothed array $F_N$:

$$I(i, j) = F_N(i, j) + \sum_{n=1}^{N} W_n(i, j). \quad (9)$$

A further step is to consider a multi-scale object representation, which associates an object contained in the data with a volume in the multi-scale transform. This representation requires the application of a segmentation method scale by scale. A general idea for object definition lies in the connectivity property. An object is located in a physical region, and the pixels of its region are connected to other significant adjacent pixels. This connectivity is present both in the same scale and in the contiguous scales. This is exactly what the MVM (Bijaoui & Rué 1995) does.

These are the steps that the MVM follows.

(i) The WT with the 'à trous' algorithm is applied to an image.
(ii) A scale-by-scale thresholding procedure is performed, obtaining the object segmentation at each scale.
(iii) In order to define the object structure, an inter-scale connectivity graph is established.
(iv) An object identification procedure extracts each connected sub-graph and considers them as objects.
(v) Finally, from each set of pixels an image of the object can be reconstructed using some reconstruction algorithms.

So, at each scale the so-called significant wavelet coefficients (values in a wavelet scale above a given detection limit usually dependent on the noise model) are searched. At each scale we have a Boolean image with pixel intensity equal to 1 when a significant coefficient has been detected, and 0 otherwise. Afterwards the segmentation is applied by labelling the Boolean values (each group of connected significant coefficients gets a different label). An inter-scale relation between two labelled zones in two adjacent scales exists if the maximum significant coefficient of the first one lies into the region of the second one in the next scale. Therefore, an object is defined as a set of inter-scale relations having a graph structure. A representation of this inter-scale connectivity graph is shown in Fig. 5.

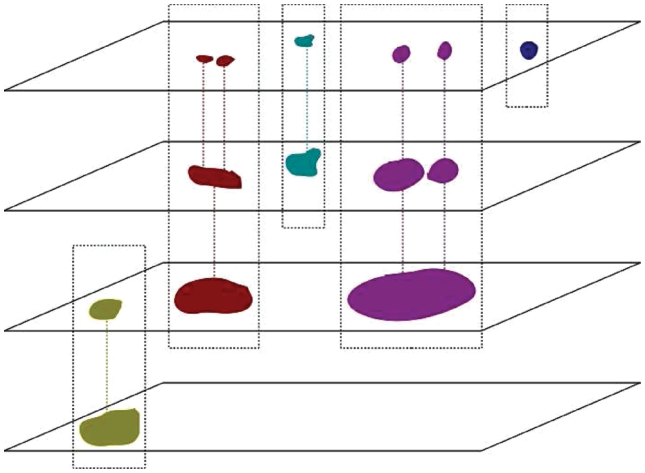

**Figure 5.** An example of the connectivity in the wavelet scales. Adjacent significant coefficients in a scale and between contiguous scales are considered part of the same object.

This pipeline and similar ones based on WT have been used as reference work in a lot of subsequent multi-scale approaches. For example, after applying a Gaussian fitting and a median filter Damiani et al. (1997) applied the MHWT to the image and local peaks over a significant threshold were considered as sources if their amplitude was significant with respect to the expected fluctuations of the local background. Very similar to this approach is the one by Freeman et al. (2002). It differs in the background estimation, since they carried this step out at each wavelet scale by an average filter and weighting the resulting values with the negative wings of the MHWT. In addition, they proposed a post-processing step that analysed some properties of the detected sources and rejected the ones that were considered as spurious.

Like Bijaoui and Rué, Starck et al. (1999) used the MVM to decompose the signal into its main components. Moreover, Broos et al. (2010) recently developed a wavelet-based strategy to find sources in X-ray images from the *Chandra* telescope. The image was deconvolved using the WT and reconstructed again to smooth the PSF effects [using a reconstruction algorithm called Richardson–Lucy (Richardson 1972; Lucy 1974) which is explained in detail in Broos et al. (2010)]. A candidate list of sources was created by locating peaks in the reconstructed image, and if those peaks fulfilled a number of properties, they were considered as sources; otherwise they were rejected.

Nevertheless, the whole MVM process is not required. Executing the detection process in only a few scales instead of in all may often be enough. In the work of Kaiser et al. (1995), the source positions and sizes were simply identified by locating peaks at their scales of maximum significance. Vielva et al. (2003) deconvolved all-sky surveys with the spherical Mexican hat wavelet transform and

proposed to divide the image in different regions, estimating the optimal scale at each region. González-Nuevo et al. (2006) also decided to apply some extensions of the MHWT to radio maps. They proposed using the Mexican hat wavelet family (MHWF; a range of MHWT obtained by applying another Laplacian operator to the MHWT, and repeating this process iteratively) to detect point sources by selecting the optimal scales of different MHWT of the family (they tested the first four members of the family.). They finally applied a local peak detection. In a similar way, Starck et al. (2009) used the MSVST and a thresholding was computed in those scales with significant wavelet coefficients to finally reconstruct the image. Lazzati et al. (1999) used only a few predefined scales where a thresholding was applied, and afterwards, the detection at different scales was correlated to remove multiple detections of the same sources and to determine which nearby sources were extended ones.

Another way to deal with WT is detecting the objects in specific scales according to the detection purpose. During the last few years, Peracaula et al. (2009b, 2011) have selected different scales depending on whether the sources to search were extended or point-shaped. As we already mentioned, depending on the type of sources, they appear in lower or higher scales. First, Peracaula et al. (2009b, 2011) computed a thresholding to the raw image to detect the brighter point sources, and they generated two images: a residual image in which bright sources were substituted by local noise, and a binarized image with the bright sources. A WT was then applied to the residual image and different strategies were followed according to the sources to be found. On the one hand, Peracaula et al. (2009b) tried to identify faint point sources, and decided to use the first three wavelet scales (the higher spatial frequency scales). On the other hand, Peracaula et al. (2011) tried to find extended structures, so they focused on the detection in the last wavelet scales (the lower spatial frequency scales). In both cases, the selected scales were thresholded, and a binary image was reconstructed from the addition of the binarized scales (in the first case the binary image with the extracted bright sources was also added with the purpose of detecting both bright and faint sources).

#### *3.1.4 Other detection criteria*

Although most of the classical approaches are based on thresholding and local peak search, other strategies have also been used to detect astronomical objects. In many cases these approaches have been developed during the last few years and are more focused on techniques from the computer vision and machine learning fields.

For example, Andreon et al. (2000) turned the object detection problem into a classification one. They classified the pixels as if they belonged to the class object or to the class background. This task was achieved using a kind of neural network (so they named this package NExt, from NEural Extractor): principal component analysis neural networks (PCA-NN) to reduce the dimensionality of the input data by eigenanalysis (basically selecting the principal vectors). They trained a PCA-NN with patches of the representative zones of the image, and a vector with less features than the input one returned. Afterwards, this output became the input of an unsupervised neural network, which was responsible for classifying the pixels between the object and the background. Based on this detection approach, Liu et al. (2003) proposed to change the PCA-NN used by Andreon et al. (2000) to local principal component analysis (a kind of PCA that clusters the input data and finds the principal vectors for each cluster). They used local PCA to automatically extract features of the image. A clustering process was then computed, and the pixels were classified from these clusters.

Aptoula et al. (2006), after the application of morphological operations, segmented the image with the 'watershed transform'. Note that in this case the images contained only one object to segment, mainly galaxies. This unsupervised segmentation acts as a drop of water falling on a topographic relief corresponding to the image (every grey level may be considered as a height in the relief). Placing a water source in each regional minimum, the relief is flooded from sources, and barriers are built when different sources are going to merge. To avoid over-segmentation, they only considered a few marked minimums as water sources. Specifically, two markers were used: one in the centre of the object and another in a minimum external region (these two markers were found by thresholding and morphological techniques). Hence, a good segmentation between object and background was computed.

Peracaula et al. (2009a) recently defined a contrast radial function (that relates the central pixel intensity with the mean of its neighbour's intensity in a given radius) in different radial distances. First, a low local thresholding was computed to the raw image and a first degree polynomial of the contrast radial function was fit to each pixel with intensities over the threshold. The goodness of the fit was given by the slope of the polynomial. Groups of at least four connected pixels with a slope larger than a certain threshold were considered as objects.

In a different way, Perret et al. (2010) recently used connected component trees (CC-trees) to detect sources in multi-band images. CC-trees have become popular models for the analysis of grey-scale images (the authors used an extension for multi-band images.) since they provide a hierarchical representation of images that can be used for segmentation and object detection, among others. The representation of a grey-scale image is based on the thresholding between its minimum and maximum grey levels (thresholding the image at different levels starting from the minimum value and increasing it until the maximum value is reached). There is a relationship of the inclusion between components at sequential grey levels in the image. The root is the whole image and at every level of the tree, the different foreground regions are decomposed in some regions obtained with a higher threshold. Perret et al. equipped the nodes with some attributes (multi-spectral information of the thresholded region), and then pruned the ones considered as irrelevant, to finally reconstruct the image. Therefore, the remaining nodes at significant levels were considered as sources.

## 4 RESULTS

Since many papers are not exclusively focused on astronomical object detection (such as the ones that just make catalogues of new sources found, or the ones that are more focused on computing the photometry of the found sources), in this section we present only the results of those papers that have source detection as their main objective. We describe the measures computed in these works and evaluate their performance, and we compare and discuss the results presented, pointing out the most interesting aspects. Finally, we highlight the techniques that are more appropriate for each type of astronomical image.

### 4.1 Evaluation measures

In the different papers, results have been evaluated in several ways. Nevertheless, most of them are measured to know which of the detected objects are truly objects. This validation is usually done

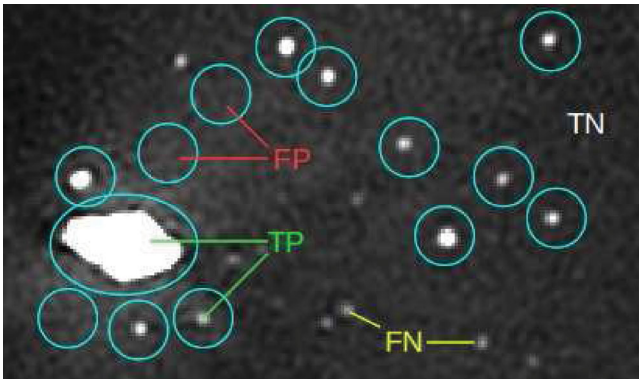


**Figure 6.** A simple example to explain TP, FP, FN and TN measures. It symbolizes the resulting image of an automated detection method. The sources detected by the method are underlined with circles.

using published catalogues or data obtained from an astronomical package used as reference (e.g. SExtractor and SAD). In some cases, the validation of the real objects is done with the assistance of an astronomical expert, who considers the detections as either true or spurious. Moreover, simulated images are widely used, since the simulated sources are placed in known positions, and therefore, it is easy to evaluate the goodness of the results by checking the detected sources that match with the previously simulated.

Whether using a reference catalogue or simulated data as ground truth, the performance of the detection (and segmentation) methods is evaluated by computing true positives (TP), false positives (FP), false negatives (FN) and true negatives (TN). TP are detections that are true sources; FP are detections that are not true sources (so they are spurious detections); FN are true sources that have not been detected (they are missed by the method, and therefore considered as background) and TN are background zones correctly considered as such. Fig. 6 shows a simple example of these different measures. Obviously, the objective is to obtain the maximum number of TP and TN, and at the same time the minimum number of FP and FN. However, in practice, increasing the number of TP usually increases the number of FP, while reducing the number of FN also reduces the number of TN. Therefore, an effort must be made to set the parameters of the detection method to maximize TP and TN and to minimize FP and FN.

Reference catalogues may also be used to directly compare the performance of the methods. As the catalogues used as references tend to be published in international journals, they have a reliable list of sources and can therefore be used to extract some measures between the reference sources and the detected ones. The two catalogues can be compared, for example, based on the sources that coincide in both catalogues or the sources that only appear in one. If in addition more reference catalogues are available, cross comparisons may be performed and the goodness of the method can be estimated by computing the number of missed sources (sources not being part of a catalogue but appearing in the rest of the catalogues).

### 4.2 Analysis of the results

We provide a qualitative comparison of the results obtained from the approaches analysed. Table 3 summarizes the evaluation measures and the catalogues or tools used as references. A qualitative evaluation of these approaches is difficult to carry out because the work has been done on different types of images and with different purposes.

Several works used TP and FP rates to evaluate the performance of their approaches. For instance, Slezak et al. (1988) first estimated by eye the different sources present in a wide field from Schmidt plates, and afterwards applied the detection method with different detection thresholds (expressed in terms of magnitude). As the magnitude threshold was decreased, the number of detected sources decreased,

**Table 3.** Summary of the results presented in the analysed articles. We show the source catalogues or the source detection packages used as reference (second column), the type of the used images and if they have real or simulated (sim) origin (third column), the number of detected objects (forth column), the measures used to evaluate the results (fifth column), and the performance (last column). Notice that forth and sixth columns may have more than one value. Slashes ('/') separate different experiments (as different parameter setting or different test images), while values in parentheses refer to the reference catalogues (in the same order that in second column). Value 'N/A' means 'not available'.

| Article | Reference | Image type | Detections | Measures | Performance |
|---|---|---|---|---|---|
| Slezak et al. (1988) | Manually | Optical (real) | 363 | TP | 353 |
| | | | | FP | 10 |
| Damiani et al. (1997) | MPE and WGA catalogues | X-ray (real) | 453 | Missed | 10 (75,47) |
| Starck et al. (1999) | N/A | Mid-infrared (sim) | 46 | TP | 45 |
| | | | | FP | 1 |
| Andreon et al. (2000) | SExtractor | Multi-band (real) | 2742/3776 | TP | 2059/2310 (2388) |
| | | | | FP | 683/1466 (1866) |
| Freeman et al. (2002) | MPE and WGA catalogues | X-ray (real) | 148 | Coincidences | 81 (12,27) |
| Perret et al. (2008) | Manually | Multi-band (real) | 17 | Recall (per cent) | 82/87 per cent |
| Peracaula et al. (2009a) | Reference catalogue (SAD) | Radio (real) | 83 | TP | 70 (68) |
| | | | | FP | 13 (33) |
| Peracaula et al. (2009b) | Reference catalogue (SAD) | Radio (real) | 86 | TP | 71 (68) |
| | | | | FP | 15 (33) |
| Guglielmetti et al. (2009) | Wavdetect | X-ray (sim) | 100 | TP | 64/41/25 (56/37/23) |
| | | | | FP | 8/9/0 (4/1/1) |
| Carvalho et al. (2009) | N/A | Optical (sim) | N/A | TP (per cent) | 67.41/56.41/82.95 per cent |
| | | | | FP (per cent) | 9.6/8.62/8.19 per cent |
| Torrent et al. (2010) | Reference catalogue (SAD and SExtractor) | Radio (real) | 601 | TP | 505 (455,473) |
| | | | | FP | 96 (474,N/A) |
| Broos et al. (2010) | Reference catalogue | X-ray (real) | 100 | TP | 89 |
| | | | | FP | 11 |

but the percentage of well-detected sources increased. The best results were obtained with a low threshold: from the 363 sources detected, 353 were TP and 10 FP. Starck et al. (1999) developed an approach for Infrared Space Observatory Camera (ISOCAM; one of the four instruments on board the *ISO – Infrared Space Observatory*) mosaics that applied to a simulation of the ISOCAM-*Hubble Deep Field*-North, detecting 45 sources from the 46 generated (which means TP = 45 and FN = 1). Andreon et al. (2000) tested several types of neural networks to a field from the Canadian Astronomy Data Centre. This field has been widely studied, so as a reference they take a specific published catalogue that consists of 4819 objects (with ∼2400 too faint to be visible). The best tests found 2742 and 3776 sources in the field, among which 2059 and 2310 were TP and 683 and 1466 were FP, respectively. Moreover, they applied the detection tool of the SExtractor package to the same field, obtaining a catalogue with 4254 sources, with 2388 TP and 1866 FP. Although SExtractor detected more sources (a number of sources similar to the one found by the reference catalogue), the absolute number of TP computed by Andreon et al. was slightly lower than SExtractor TP, and in the FP case, they were substantially lower.

More recently, Peracaula et al. (2009a, 2011) tested their approaches on a deep radio map obtained by the Giant Metrewave Radio Telescope (GMRT). They compared their results with a reference catalogue that detected 101 sources (68 TP and 33 FP). These approaches presented similar results, and both outperformed the reference values (especially in terms of FP). In Peracaula et al. (2009a) they found 70 TP and 13 FP, whereas in Peracaula et al. (2011) they found 71 TP and 15 FP. Torrent et al. (2010) also used a radio map of the GMRT, but one covering a more extended region of the sky. They applied their method and the sad and SExtractor detection tools to the image, and compared the sources detected to a reference catalogue. Their approach achieved better results than sad and SExtractor. While sad obtained 455 TP and 474 FP, and SExtractor 473 TP (the number of FP was not available), they found 505 TP and 96 FP.

Guglielmetti et al. (2009) performed experiments using simulated images with 100 sources and repeated them adding different levels of noise: 0.1 per cent, 1 per cent and 10 per cent of the counts, respectively. The obtained results were 64, 41 and 25 TP, and 8, 9, and 0 FP, respectively, showing that increasing the level of noise, the number of detections became lower, although all the detections were TP (these results illustrate the importance of defining if the priority of the detection strategy is to find the maximum number of true sources regardless of the number of spurious detections, or otherwise is to guarantee that most of the detections are true regardless of missing true sources). Therefore, in terms of TP, Guglielmetti et al. obtained better results than Wavdetect, but not with FP. Carvalho et al. (2009) also used three simulated images (the first two with 16 objects and the last one with eight objects). Their method was able to detect (in percentages) 67.41 per cent, 56.41 per cent and 82.95 per cent of the simulated sources (TP), and obtained 9.6 per cent, 8.62 per cent and 8.19 per cent of spurious detections (FP). They also estimated the performance of their method by an error computed by adding the number of FP and FN (42.19 per cent, 52.2 per cent and 25.15 per cent, respectively).

Other works have used different ways to estimate their results. For instance, Damiani et al. (1997), in order to compare the performance of their method on seven images of the *ROSAT* satellite, used two published catalogues called MPE (286 sources in total) and WGA (389 sources in total) as reference, and counted the number of sources detected by two catalogues and missed by the other one. Their method detected 453 sources (244 coincidence with MPE, 272 coincidence with WGA and 197 sources present in all catalogues). They found that their method missed 10 sources, less than MPE and WGA, which missed 75 and 47 sources, respectively. Freeman et al. (2002) also used crossed comparisons between the sources found with their method in a *ROSAT* image and the ones found by MPE (100 sources found) and WGA (127 sources found). They found 148 sources, of which 81 appear in all three catalogues. The coincidences between their work and MPE were 97, while the coincidences with WGA were 108 (the coincidences between MPE and WGA were 84). Broos et al. (2010) tested their local peak method in combination with Wavdetect to find 100 sources (50 with Wavdetect and 50 with their source detection method) in a map from the *Chandra X-ray Observatory*. They compared these sources with a reference catalogue and found 89 coincidences. Perret et al. (2008) had a reference catalogue with nine galaxies detected. To validate the good performance of their galaxy-finding method, first, they tested their method on two images, and found 17 objects: six galaxies of the reference catalogue, eight new sources that an expert also considered to be galaxies and three FP. It means a recall (percentage of true detected galaxies) of 82 per cent. Testing the method on 16 images they found a recall of 87 per cent.

In some works, the performance depends on the selected parameter setting. For instance, Vielva et al. (2003) and González-Nuevo et al. (2006) repeated several experiments with different thresholds until they got a rate of spurious sources lower than the 5 per cent of the total number of sources detected. Moreover, these two approaches worked with images with several frequency channels, and therefore, a different threshold was needed at each channel. Vielva et al. used all-sky maps with 10 channels, and for example, in the three lower channels they obtained 27257, 5201 and 4195 sources, respectively. González-Nuevo et al. also performed this strategy in an image with three frequency channels, and for each channel they applied the first four transforms of the MHWF. For example for the channel with lower frequency the sources detected were 543, 639, 583 and 418, respectively.

## 5 DISCUSSION

As we have seen, several strategies are used to deal with the astronomical source detection problem. Most of them coincide in focusing the detection criteria on the intensity of the image pixels, whether in the image transformation steps in order to enhance the sources with respect to the background, or in the detection process, choosing those pixels with an intensity value suggesting they are likely to be part of an object. We have seen that all the different image transformation and detection steps are used indistinctly in all types (all frequency bands) of astronomical images, although there are techniques that are more commonly used in some particular bands. An overview of the different techniques reviewed with their strengths and weaknesses is presented in Table 4.

Regarding the astronomical images, two main drawbacks caused by the acquisition process hinder detection: the variable background and the noise. Hence, image transformation steps have taken a fundamental role in astronomical image processing. Therefore, some image transformation steps must be applied depending on whether the images have background variations, noise or both. Background inhomogeneity can be corrected by applying a smoothing with filters or by removing the background. In many cases background subtraction is preferable to filtering, because implicitly it is already detecting sources by discarding those regions that with high probability are not sources. Furthermore, although filtering decreases the impact of background variations (and also noise), it may blur the

**Table 4.** Overview of the different techniques reviewed with their advantages and drawbacks.

| Step | Description | Strengths | Weaknesses |
|---|---|---|---|
| Image transformation | | | |
| Basic image transformations | Basic transformation steps such as filtering, profile fitting or morphological operators | Intuitive, fast and easy<br>Slightly emphasize sources<br>Correct background variations<br>Filter noise | Limited<br>May blur and twinkle the image<br>Often needs more transformation steps |
| Bayesian approaches | Methodologies based on Bayesian inference | Emphasize sources<br>Good results with source variability<br>Reduce background variability and filter noise | Computational cost<br>Need prior knowledge |
| Matched filtering | Methods based on filters with the profile of the objects to find | Rather emphasize sources<br>Reduce background variability and filter noise | Need prior knowledge<br>Different filters required for different sources |
| Multi-scale approaches | Approaches that decompose the image in several scales | Filter noise and delete background (same time)<br>Good results with source variability<br>Allow working with different scales<br>Implicitly performs source detection<br>Can deblend sources | Quite slow<br>Often needs combinations of transforms |
| Detection criterion | | | |
| Thresholding | Pixels above a certain threshold are considered as part of the object | Good results with all sources<br>Good results with inhomogeneous background<br>Good results with significant contrast and high SNR | Difficult to select the optimal threshold<br>Not suitable for faint sources |
| Local peak search | Search pixels that are maximums in a neighbourhood | Good results with point sources<br>Good results with noisy images | Need an additional detection process<br>Not suitable for extended sources |
| Other methods | Other innovative detection methods | Similar results than the other two methods | Still not have enough acceptance |

sources. In the case of noise, filtering seems to be the most widely used technique (Mighell 1999; Makovoz & Marleau 2006; Perret et al. 2008; Yang et al. 2008).

Multi-scale approaches are also gaining popularity because they allow background to be removed and noise to be filtered at the same time (more advantages are shown in Table 4). Since they extract the signal at different scales, they are suitable when the images have sources with different sizes and complex shapes. Furthermore, being able to work with multiple scales (and therefore multiple images), this technique offers the possibility of extracting the best of each one, or selecting the better suited scales to perform the detection. Most multi-scale analyses are based on the WT or variants of it (Damiani et al. 1997; Starck et al. 1999; Freeman et al. 2002; Vielva et al. 2003; González-Nuevo et al. 2006; Peracaula et al. 2009b).

Analysing more particularly the use of the image transformation methods at the different frequency bands, we observe that basic image transformation is commonly applied to optical and multi-band images, which means that this kind of method has a good performance in the visible band and its close frequencies (although we also find basic techniques combined with the other frequency bands, even though to a lesser extent). In contrast, approaches that work with optical and multi-band images are not based on a multi-scale decomposition. The multi-scale strategies are widely applied to radio, infrared and X-ray images. We have also noticed that matched filtering is especially used in the radio band, while Bayesian approaches are equally applied to different bands.

Regarding the detection criteria, the vast majority of works reviewed used thresholding and local peak search, and both methods seem to have a similar performance. We have seen that after any kind of image transformation, both methods are used interchangeably and equally for all types of images. However, the choice may depend on some characteristics as can be seen in Table 4. Local peak search is not suitable for detecting extended sources, and it is preferable when images are noisy and have point sources, since it is a neighbourhood-based algorithm and easily discards noise pixels (avoiding confusion with source pixels). When an image has an inhomogeneity background, the best choice is to tackle the detection with local thresholding, whereas global thresholding is preferable when an image has significant contrast with objects and background or a high SNR. The rest of the approaches that do not use either thresholding or local peak search have in common that they are relatively recent (most of them developed in the last years), they are all innovative and they perform object detections on a par with the two typical methods.

Analysing the results, we noticed that the best performances in terms of TP were obtained by Slezak et al. (1988), Starck et al. (1999), Peracaula et al. (2009a, 2011) and Torrent et al. (2010). Moreover, Damiani et al. (1997) and Freeman et al. (2002) also obtained satisfactory results in terms of coincidences with published catalogues. Some other works obtained good results, but we consider that the selected ones are more significant because they dealt with considerable amounts of sources (in most cases hundreds of them) and did not use additional resources as astronomical detection packages. We want to stress, on the one hand, that most of the approaches that apply any kind of image transformation used multi-scale strategies, specifically the WT (Damiani et al. 1997; Peracaula et al. 2009b; Starck et al. 1999; Freeman et al. 2002). On the other hand, the detection step used is mostly thresholding (Slezak et al. 1988; Peracaula et al. 2009b; Starck et al. 1999; Freeman et al. 2002) [the other detection criteria used were innovative methods

such as contrast radial function and boosting in the approaches of Peracaula et al. (2009a) and Torrent et al. (2010), and a local peak search in the Damiani et al. (1997) approach].

## 6 CONCLUSIONS

This paper has reviewed automated approaches to source detection in astronomical images, classifying them according to the type of image transformation and the detection criterion used. In addition, the results obtained by these approaches have been summarized and compared, and the most frequently used evaluation measures in this field have been reviewed. We observed that the automated detection of objects in astronomical images is a challenging task due to the huge amount of objects in the sky and the limitations of the capture devices.

The different methods reviewed have advantages and disadvantages and using either one or another will depend on the features of the images and the aim. There are several factors to take into account such as noise, dynamic range, interferences, variable background, source shapes, etc. Moreover, the different methods need to be tuned to provide optimum results.

Astronomical source detection is a broad topic, and each type of astronomical image could be analysed separately. For this reason, in future work, we want to perform an analysis for the different image types, highlighting the main features that make some strategies more suitable at each frequency band.

## ACKNOWLEDGMENTS

This work has been supported by Grant AYA2010-21782-C03-02 from EMCI-Ministerio de Ciencia e Innovación. MM holds an FI grant 2011FI_B 00081. The authors would like to thank the anonymous referee for valuable comments which have improved the paper.

## REFERENCES

Andreon S., Gargiulo G., Longo G., Tagliaferri R., Capuano N., 2000, MNRAS, 319, 700
Aptoula E., Lefèvre S., Collet C., 2006, in Proc. EUSIPCO, Mathematical Morphology Applied to the Segmentation and Classification of Galaxies in Multispectral Images
Barreiro R. B., Sanz J. L., Herranz D., Martínez-González E., 2003, MNRAS, 342, 119
Belbachir A. N., Goebel P. M., 2005, in Proc. SSP, A Combined Multiresolution Approach for Faint Source Extraction from Infrared Astronomical Raw Images Sequence. IEEE, p. 459
Bertalmio M., Sapiro G., Caselles V., Ballester C., 2000, in Akeley K., ed., in Proc. ACM SIGGRAPH Conf. on Computer Graphics, Image Inpainting. ACM Press/Addison-Wesley Publishing Co., New York, p. 417
Bertin E., 2001, in Banday A. J., Zaroubi S., Bartelmann M., eds, Mining the Sky, Mining Pixels: The Extraction and Classification of Astronomical Sources. Springer-Verlag, Berlin, p. 353
Bertin E., Arnouts S., 1996, A&AS, 117, 393
Bijaoui A., 1980, A&A, 84, 81
Bijaoui A., Rué F., 1995, Signal Processing, 46, 345
Bijaoui A., Guennec A., Benoist C., Slezak E., 2005, in Truchetet F., Laligant O., eds, Proc. SPIE Vol. 6001, Wavelet Applications in Industrial Processing III. SPIE, Bellingham, p. 1
Broos P. S., Townsley L. K., Feigelson E. D., Getman K. V., Bauer F. E., Garmire G. P., 2010, ApJ, 714, 1582
Buonanno R., Buscema G., Corsi C. E., Ferraro I., Iannicola G., 1983, A&A, 126, 278
Candès E. J., Donoho D. L., 1999, Phil. Trans. R. Soc. Lond. A, 357, 2495
Candès E. J., Donoho D. L., 2000, in Aldroubi A., Laine A. G., Unser M. A., eds, Proc. SPIE Vol. 4119, Wavelet Applications in Signal and Image Processing VIII. SPIE, Bellingham, p. 1
Carvalho P., Rocha G., Hobson M. P., 2009, MNRAS, 393, 681
Criminisi A., Pérez P., Toyama K., 2004, IEEE Trans. Image Processing, 13, 1200
Damiani F., Maggio A., Micela G., Sciortino S., 1997, MNRAS, 483, 350
Feroz F., Hobson M. P., 2008, MNRAS, 384, 449
Freeman P. E., Kashyap V., Rosner R., Lamb D. Q., 2002, ApJS, 138, 185
Freund Y., Schapire R. E., 1997, J. Comput. Syst. Sci., 55, 119
Goderya S. N., Lolling S. M., 2002, Astrophys. Space Sci., 279, 377
González-Nuevo J., Argüeso F., López-Caniego M., Toffolatti L., Sanz J. L., Vielva P., Herranz D., 2006, MNRAS, 369, 1603
Graps A., 1995, IEEE Comput. Sci. Eng., 2, 50
Guglielmetti F., Fischer R., Dose V., 2009, MNRAS, 396, 165
Haindl M., Šimberová S., 1996, A&AS, 115, 189
Hanson K. M., 1993, in Loew M. H., ed., Proc. SPIE Vol. 1898, Medical Imaging 1993: Image Processing. SPIE, Bellingham, p. 716
Haupt J., Castro R., Nowak R., 2009, in Dyk D. V., Welling M., eds, Proc. AISTATS, Distilled Sensing: Selective Sampling for Sparse Signal Recovery. JMLR: W&CP 5, p. 216
Herranz D., López-Caniego M., Sanz J. L., González-Nuevo J., 2009, MNRAS, 394, 510
Herzog A. D., Illingworth G., 1977, ApJS, 33, 55
Hobson M. P., McLachlan C., 2003, MNRAS, 338, 765
Hopkins A. M., Miller C. J., Connolly A. J., Genovese C., Nichol R. C., Wasserman L., 2002, AJ, 123, 1086
Irwin M. J., 1985, MNRAS, 214, 575
Jarvis J. F., Tyson J. A., 1981, AJ, 86, 476
Kaiser N., Squires G., Broadhurst T., 1995, ApJ, 449, 460
Kron R. G., 1980, ApJS, 43, 305
Lang D., Hogg D. W., Mierle K., Blanton M., Roweis S., 2010, AJ, 139, 1782
Lazzati D., Campana S., Rosati P., Panzera M. R., Tagliaferri G., 1999, ApJ, 524, 414
Le Fèvre O., Bijaoui A., Mathez G., Picat J. P., Lelièvre G., 1996, A&A, 154, 92
Liu Z., Chiu K., Xu L., 2003, Neural Networks, 16, 437
López-Caniego M., Herranz D., Sanz J. L., Barreiro R. B., 2005, EURASIP J. Appl. Signal Processing, 15, 2426
Lucy L. B., 1974, AJ, 79, 745
Makovoz D., Marleau F. R., 2006, PASP, 459, 341
Melin J. B., Bartlett J. G., Delabrouille J., 2006, A&A, 117, 1113
Mighell K. J., 1999, in Mehringer D. M., Plante R. L., Roberts D. A., eds, ASP Conf. Ser. Vol. 172, Astronomical Data Analysis Software and Systems XVIII. Astron. Soc. Pac., San Francisco, p. 317
Newell B., O'Neil E. J., Jr, 1977, PASP, 89, 925
Otsu N., 1979, in Trans. SMC, Vol. 9, A Threshold Selection Method from Gray-Level Histograms. IEEE, p. 62
Peracaula M., Freixenet J., Lladó X., Martí J., Paredes J. M., 2009a, in Bohlender D., Durand D., Dowler P., eds, ASP Conf. Ser. Vol. 411, Astronomical Data Analysis Software and Systems XVIII. Astron. Soc. Pac., San Francisco, p. 255
Peracaula M., Martí J., Freixenet J., Martí J., Paredes J. M., 2009b, in Araujo H., Mendonça A. M., Pinho A. J., Torres M. I., eds, Lect. Notes Comput. Sci., Vol. 5524, Pattern Recognition and Image Analysis. Springer-Verlag, Berlin, p. 192
Peracaula M., Oliver A., Torrent A., Lladó X., Freixenet J., Martí J., 2011, in Macq B., Schelkens P., eds, IEEE Int. Conf. Image Processing, Segmenting Extended Structures in Radio Astronomical Images by Filtering bright Compact Sources and using Wavelets Decomposition. IEEE, p. 2861
Perret B., Lefèvre S., Collet C., 2008, Pattern Recognition, 42, 470
Perret B., Lefèvre S., Collet C., 2010, in Proc. ICPR, Connected Component Trees for Multivariate Image Processing and Applications in Astronomy. IEEE, p. 4089

Richardson W. H., 1972, J. Opt. Soc. America, 62, 55
Savage R. S., Oliver S., 2007, ApJ, 661, 339
Slezak E., Bijaoui A., Mars G., 1988, A&A, 201, 9
Starck J.-L., 2002, in Bohlender D. A., Durand D., Handley T. H., eds, ASP Conf. Ser. Vol. 281, Astronomical Data Analysis Software and Systems XI. Astron. Soc. Pac., San Francisco, p. 391
Starck J.-L., Bobin J., 2010, in Trew R. J., Brittain J. E., eds, Proc. IEEE. Astronomical Data Analysis and Sparsity: From Wavelets to Compressed Sensing. Vol. 98, IEEE, p. 1021
Starck J.-L., Murtagh F., 2006, Astron. Astrophys. Libr., Astronomical Image and Data Analysis, 2nd edn. Springer-Verlag, Berlin
Starck J.-L., Aussel H., Elbaz D., Fadda D., Cesarsky C., 1999, A&AS, 138, 365
Starck J.-L., Donoho D. L., Candès E. J., 2003, A&A, 398, 785
Starck J.-L., Fadili J. M., Digel S., Zhang B., Chiang J., 2009, A&A, 504, 641
Stetson P. B., 1987, PASP, 99, 191
Szalay A. S., Connolly A. J., Szokoly G. P., 1999, AJ, 117, 68
Torrent A., Peracaula M., Lladó X., Freixenet J., Sánchez-Sutil J. R., Martí J., Paredes J. M., 2010, in Proc. ICPR, Detecting Faint Compact Sources using Local Features and a Boosting Approach. IEEE, p. 4613
Vielva P., Martínez-González E., Gallegos J. E., Toffolatti L., Sanz J. L., 2003, MNRAS, 344, 89
Vikhlinin A., Forman W., Jones C., Murray S., 1995, ApJ, 451, 542
Yang Y., Li N., Zhang Y., 2008, in Proc. SMC, Automatic Moving Object Detecting and Tracking from Astronomical CCD Image Sequences. IEEE. p. 650
Zhang C. Y., 1995, in Shaw R. A., Payne H. E., Hayes J. J. E., eds, ASP Conf. Ser. Vol. 77, Astronomical Data Analysis Software and Systems IV. Astron. Soc. Pac., San Francisco, p. 514
Zhang Y., Luo A., Zhao Y., 2004, in Quinn P. J., Bridger A., eds, Proc. SPIE Vol. 5493, Optimizing Scientific Return for Astronomy Through Information Technologies. SPIE, Bellingham, p. 521

This paper has been typeset from a TEX/LATEX file prepared by the author.